



RESEARCH ARTICLE

Design and experiment of a pneumatic self-repairing soft actuator

Zhaoyu Liu¹, Yuxuan Wang¹ , Shaoke Yuan¹ and Yanqiong Fei^{1,2,*} 

¹Research Institute of Robotics, Shanghai Jiao Tong University, Shanghai, China and ²Shenzhen Research Institute, Shanghai Jiao Tong University, Shenzhen, China

*Corresponding author. E-mail: fyq_sjtu@163.com

Received: 19 October 2022; **Revised:** 12 January 2023; **Accepted:** 19 January 2023; **First published online:** 14 February 2023

Keywords: soft actuator, self-repairing, pneumatic, structural optimization

Abstract

This paper presents a study on the design and modeling of a novel pneumatic self-repairing soft actuator. The self-repairing soft actuator is composed of driving element, heating element, and repairing element. The driving element completes the deformation of the self-repairing soft actuator. The heating element and the repairing element complete the self-repairing function of the self-repairing soft actuator. A model used to optimize the structure is established, and the structure of the self-repairing soft actuator is determined through finite element analysis and experiment. The self-repairing time model of the soft actuator is established. The influences of different factors on the self-repairing effect and the self-repairing time are analyzed. The self-repairing scheme of the soft actuator is determined. Experiments show that the shortest time for the self-repairing soft actuator to complete the self-repairing process is 83 min. When the self-repairing soft actuator works normally, the bending angle can reach 129.8° and the bending force can reach 24.96 N. After repairing, the bending angle can reach 108.2°, and the bending force can reach 21.85 N. The repaired soft actuator can complete normal locomotion.

1. Introduction

The soft robot is made of flexible materials, which can change its shape and size arbitrarily within a large range. Due to the softness of the materials, soft robots have excellent environmental adaptability and flexibility [1, 2]. Soft robots can imitate the locomotion of animals in nature, realize the special locomotion in complex environments, and adapt to environments that humans cannot reach to expand the field of human exploration [3–7].

In recent researches, various soft bionic robots have been developed [8–13]. These soft bionic robots can imitate the behavior of animals in the environment. The soft snake-like robot can simulate the snake to meander [14]. The soft biomimetic fish robot can imitate the swimming behavior of the fish in water [15]. The bioinspired quadrupedal robot can mimic the gait of quadruped animals [16]. Some animals, such as gecko and octopus, can heal themselves after injury (such as gecko stagnation) [17]. For the soft bionic robot, the high compliance makes its structure prone to perforation and breakage [18]. When the pneumatic soft bionic robot moves or works in the environment, the contact between the actuating part and sharp objects may cause damage such as air leakage or overpressure [19]. Therefore, it is particularly important to add materials with self-repairing characteristics to the structure of soft bionic robot to make it have self-repairing function. With the advent of self-repairing materials, it is possible for soft robots to achieve self-repairing function after damaged in the work. The self-repairing material can improve the mechanical strength, fracture toughness, and corrosion resistance of the damaged soft robot, so as to prolong the service life of the soft robot [20].

Self-repairing materials can be divided into different categories according to their repairing mechanism or the stimulation required for repairing. It is mainly divided into two categories: external repairing

mechanism and internal repairing mechanism [21]. The external repairing mechanism is completed by adding healing agents that are not inherent in the material structure into the reservoir. These reservoirs can be hollow fibers [22], vascular systems [23], or microcapsules [24] embedded in the material matrix. After damage, the reservoir breaks, the healing agent seeps out to close the fracture, and the mechanical properties are restored after chemical reaction. The number of healing cycles is limited due to depletion of healing agents stored in a limited capsule volume or blockage of the vascular system. Internal repairing mechanism depends on physicochemical interactions [25, 26] or reversible covalent bonds [27, 28] in its chemical structure. These chemical structures can be broken in a reversible way and modified to restore the structure and properties of the material, which usually requires appropriate stimulation, including ionic interactions [29], hydrogen bonding [30], metal-coordination ligand [31], borate ester bond [32], Diels–Alder reaction [33], aliphatic disulfide bond exchange [34], imine bond [35], etc. Whether external repairing mechanism or internal repairing mechanism, it is usually necessary to apply appropriate stimulation to make the material begin to repair [36]. The stimulation of external repairing materials is usually the damage itself, such as sharp objects puncturing the shell of the healing agent. Internal repairing materials are designed for a wide range of stimuli, the most common of which are heat [37] and ultraviolet [38].

For the current self-repairing soft robots, most of the repair process is more than 30 min [39], and some of it can take up to 24 h [40]. For the soft robots applied in some specific situations, the long repair time might reduce work efficiency.

In this study, a novel self-repairing soft actuator is designed. This self-repairing soft actuator can be applied to soft crawling robot as the body part. The self-repairing soft actuator can complete the self-repairing function after the inflation position is damaged, and the whole repairing process does not need manual operation. Compared with the existing self-repairing soft robots, this actuator can greatly shorten the time of self-repairing process.

2. Design and modeling

This section introduces the design and structural parameters of the self-repairing soft actuator. The structure of self-repairing soft actuator is established, and the optimal structure is determined by using the topology optimization function to maximize the bending angle during inflation.

2.1. Design of the self-repairing soft actuator

For the soft actuator without enclosure, the material characteristics of silicone rubber lead to large lateral expansion when the soft actuator is inflated [41]. The bending angle and bending force of the soft actuator can be effectively improved by using a structure with certain stiffness (such as fiber line and connector) to limit the lateral expansion of the soft actuator [42, 43]. Darmohammadi et al. [44] increased the bending angle and bending force of the soft actuator by installing the fiber-reinforced structure on the soft actuator. For the soft actuator, proper enclosure can improve the bending effect, while the enclosure with high redundancy will increase the stiffness of the soft actuator and reduce the bending effect of the soft actuator. Through the research on the topology optimization of the self-repairing soft actuator in Section 2.2, we have determined the structure of the self-repairing soft actuator.

The structure of the self-repairing soft actuator is shown in Fig. 1. The self-repairing soft actuator consists of three elements: driving element, heating element, and repairing element.

The driving element is made of silicone rubber (Dragon Skin 20 (Smooth-on, USA)), and its cross-section is shown in Fig. 1(b). Considering that the actuator will be applied to our soft robot in the future, we have determined the size of the actuator, as shown in Table I. The driving element has three air chambers, and the omni-directional bending locomotion in the plane can be realized through the inflation and deflation of the three air chambers. Three air pipes are connected to the end of the driving element to control the inflation and deflation of the three air chambers.

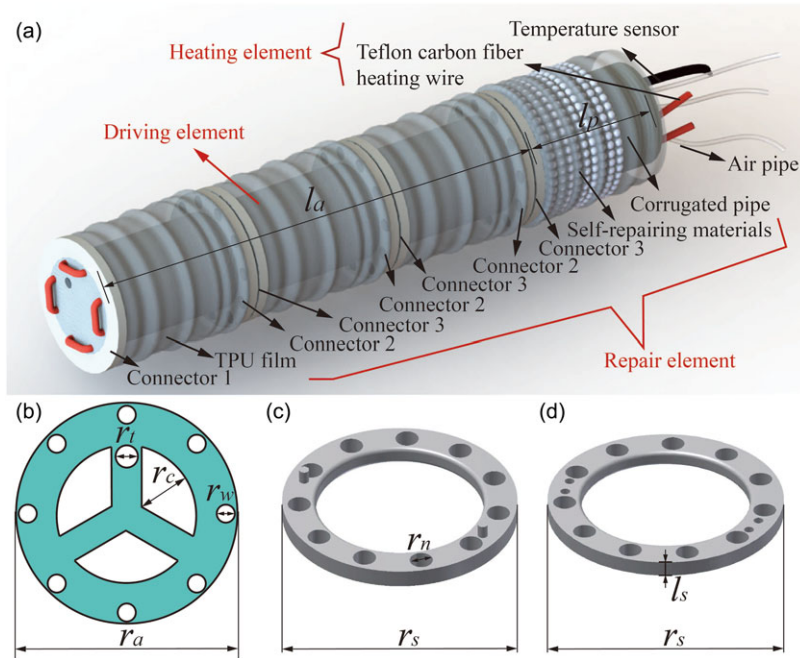


Figure 1. Schematic of self-repairing soft actuator. (a) Self-repairing soft actuator. (b) The section view of the actuator. (c) Connector 2. (d) Connector 3.

The heating element includes a Teflon carbon fiber heating wire and a temperature sensor installed inside the actuator. The Teflon carbon fiber heating wire is used to melt the self-repairing material, and the length of the heating wire is 1.6 m. The temperature sensor (XH-W3012) is used to monitor the temperature of the self-repairing materials during the self-repairing process of the actuator in real time.

The repair element includes self-repairing materials, Thermoplastic Polyurethane (TPU) film, connector 1, connector 2, connector 3, and corrugated pipe. The self-repairing materials are starch-based biomaterial particles with a diameter of less than 4.5 mm. It is used for repairing the damaged actuator. It is initially placed at the end of the actuator and wrapped by TPU film and corrugated pipe, as shown in Fig. 2. When the self-repairing soft actuator performs self-repairing function, starch-based biomaterial particles will enter the position between the actuator and the TPU film from the connector 3 at the end of the actuator. The starch-based biomaterial particles are white particles at normal atmospheric temperature and are melt into colorless fluid after external heating. The melting temperature is 70–100°C and the heating voltage is 38 V. The actuator is divided into three parts by connector 1, connector 2, and connector 3. Each part of the actuator is composed of two connectors and a piece of film. Connector 2 and connector 3 can be fixed together by rotation, so as to control the falling position of self-repairing material. The structure of connector 2 and connector 3 is shown in Fig. 1(c) and 1(d). The TPU film is made of 0.012 mm thick TPU material. There are three reasons for using TPU film: (1) TPU film has almost no weight, and TPU film is longer than the actuator, so the TPU film will not limit the deformation of the actuator when bending. (2) The TPU film can form a fixed size space (about 8 mm thick circle) between the actuator, which can fix the self-repairing material on the outside of the device. (3) When the self-repairing material melts, the TPU film can well wrap the liquid self-repairing material. The self-repairing soft actuator is shown in Fig. 2.

2.2. Structural topology optimization

For the self-repairing soft actuator, the number of connectors not only affect the bending angle and the bending force during inflation but also affect the self-repairing process. The most appropriate number of

Table I. Descriptions and symbols of the self-repairing soft actuator.

Descriptions	Symbols	Values (mm)
Length of the actuator	l_a	200
Length of the corrugated pipe	l_t	40
Height of the connector	l_s	4
Diameter of the actuator	r_a	40
Height of air chamber	r_c	10.5
Diameter of heating wire hole	r_w	3
Diameter of sensor hole	r_t	5
Diameter of connector hole	r_n	5.5
Diameter of the connector	r_s	56

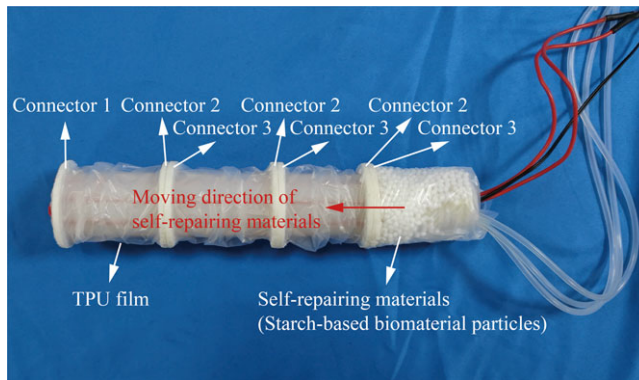


Figure 2. The self-repairing soft actuator.

connectors can be obtained through topology optimization (a design method for determining the optimal structural configuration to obtain the required performance).

In general, the optimal design of elastic structures includes information on the topology, size, and shape of the structure. The level set model allows all three problems to be solved at the same time. The structural optimization problem can be specified as ref. [45]

$$\begin{aligned}
 \min_{\Omega} \quad & Obj(u) = \int_{\Omega} F(u) d\Omega \\
 \text{subject to:} \quad & \int_{\Omega} E_i \varepsilon_i(u) d\Omega = \int_{\Omega} p v d\Omega + \int_{\partial\Omega_t} \tau v d\Omega_n, \\
 & u|_{\partial\Omega_u} = u_0 \quad \forall v \in U, \\
 & V\kappa - V_n \leq 0
 \end{aligned} \tag{1}$$

where $Obj(u)$ is the objective function. F refers to the specific physical or geometric type described. The entity domain of the structure is Ω , and its boundary is $\partial\Omega$. u is the displacement field in the space U of kinematic allowable displacement field. E_i is the elastic tensor, and ε_i is the stress tensor. p is the applied pressure, v is the virtual displacement field, and τ is the boundary traction. V and κ are the volume fraction of the enclosure and the total volume of the design domain. V_n is the maximum allowable volume of the design domain.

For silicone rubber, a hyperelastic nonlinear material, its deformation process presents obvious material nonlinearity and geometric nonlinearity. In this case, the mechanical behavior of this material is usually analyzed based on the strain energy function W . For the silicone rubber body of the self-repairing

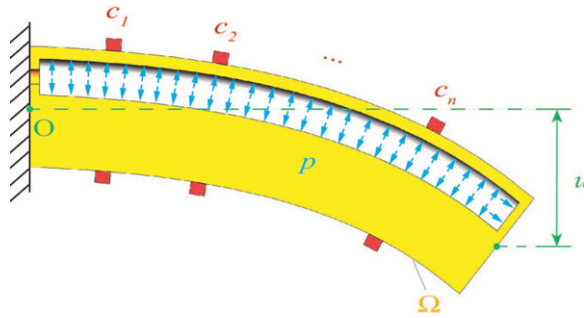


Figure 3. *Soft actuator with connectors c_n installed. Single chamber inflation for bending motion.*

soft actuator, it is assumed that the coordinate of one particle G in the configuration before deformation is x and the coordinate of the configuration after deformation is X . According to Lagrange’s point of view, x can be written as a function of X .

$$x = x(X) \tag{2}$$

Then, the deformation gradient M can be defined as

$$dx = \frac{\partial x}{\partial X} dX = MdX, \tag{3}$$

$$M = \frac{\partial x}{\partial X} = \begin{bmatrix} \frac{\partial x_1}{\partial X_1} & \frac{\partial x_1}{\partial X_2} & \frac{\partial x_1}{\partial X_3} \\ \frac{\partial x_2}{\partial X_1} & \frac{\partial x_2}{\partial X_2} & \frac{\partial x_2}{\partial X_3} \\ \frac{\partial x_3}{\partial X_1} & \frac{\partial x_3}{\partial X_2} & \frac{\partial x_3}{\partial X_3} \end{bmatrix}, \tag{4}$$

By referring to the generalized neo-Hookean model [46], the elastic properties of silicone rubber can be expressed by strain energy function W

$$W = \frac{\mu}{2} (tr(MM^T) - 3) + \frac{1}{D} (J - 1)^2, \tag{5}$$

where μ is the shear modulus of the material, J is the elastic volume ratio, and D is the coefficient to measure incompressibility. Referring to the structural optimization theory in Eq. (1), a similar structural optimization model can be obtained

$$\begin{aligned} \min_{\Omega} \quad & Obj(u) \\ \text{subject to:} \quad & K(u) U(u) = F, \\ & V_{\kappa} - V_n \leq 0 \end{aligned} \tag{6}$$

where $K(u)U(u) = F$ is the equilibrium equation due to boundary conditions and constraints. K is the stiffness matrix and U is the displacement matrix. V and κ are the volume fraction of the enclosure and the total volume of the design domain. V_n is the maximum allowable volume of the design domain.

For the self-repairing soft actuator, three air chambers can realize the omni-directional bending locomotion of the actuator in the plane. Therefore, the designed structure should meet the maximum omni-directional bending angle. Since the shape and the size of the connector of the self-repairing soft actuator are determined, the shape optimization can be ignored in structural topology optimization. For size optimization, that is, the change of volume fraction of the enclosure V can be transformed into the change of connector number c_n . As shown in Fig. 3, we fixed one end of the soft actuator and inflated one of the air chambers.

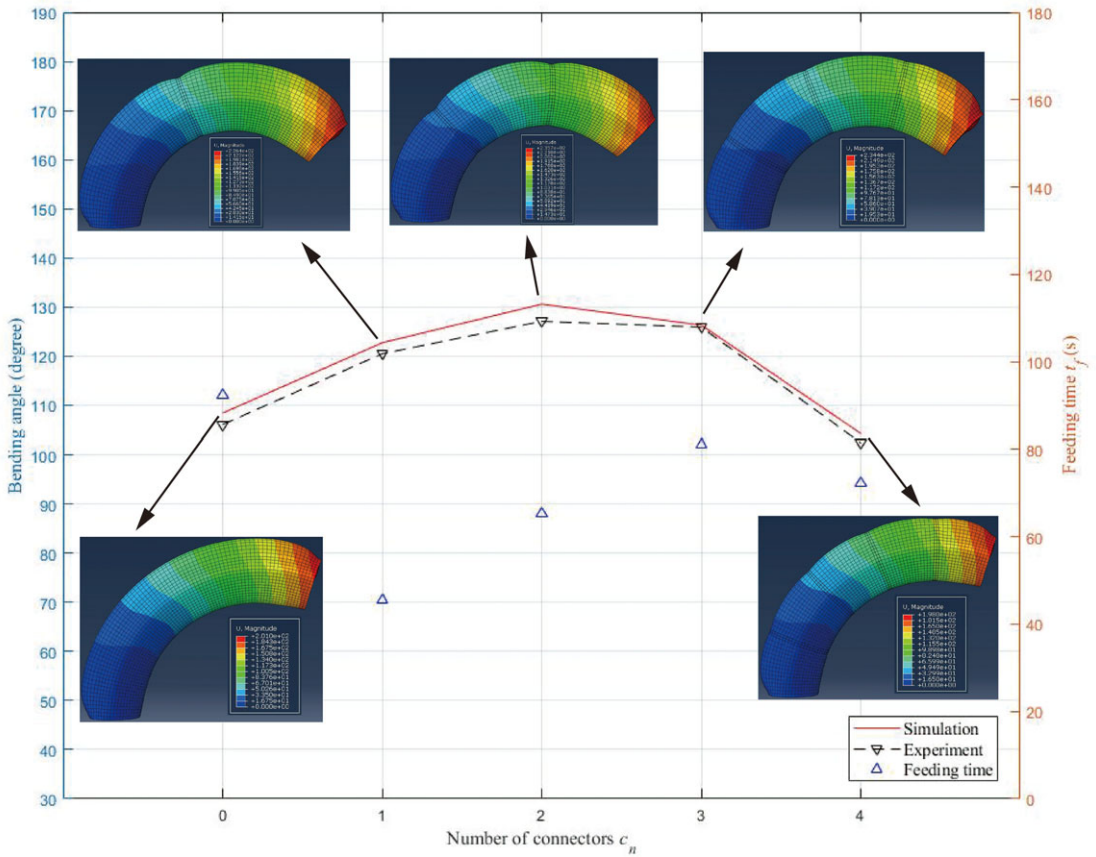


Figure 4. The optimal solution depends on the number of connectors c_n . The deformed shapes at 90 kPa are plotted as an insets.

The finite element simulated bending state of the soft actuator is compared with the experimental bending state. When Abaqus is used for analysis, C3D8H element (eight-node linear tetrahedron and hybrid element) is used to describe silicone rubber, and shell element (S3) is used to describe connector. Because the connectors and silicone rubber have good interaction characteristics, it has good convergence. It can be seen from Fig. 4 that the experimental data are basically consistent with the simulation data. The small error is mainly caused by the difference between the simulated gravity parameters and the actual gravity parameters in the experimental environment.

Figure 5 shows the air inflation bending experiment when the number of installed connectors of the actuator is different. In Fig. 5(a), the actuator is fixed on the susceptor, and the inflation pressure is 0 kPa. In Fig. 5(b–f), the actuator is divided into segments A according to the number of connectors. When the inflation pressure is 90 kPa, the bending angle of the actuator is tested. Finally, the feeding time t_f required for the self-healing material to enter segment A₁ when the number of connectors is different and the actuator is not inflated is obtained through experiments.

From Figs. 4 to 5, it can be seen that when the number of connectors is 2, the bending angle of the self-repairing soft actuator is the largest, which is 129.8°. At this time, the feeding time t_f of the self-repairing material is 65.4 s. Considering that the feeding time t_f of self-repairing materials can be shortened as much as possible without affecting the performance of the self-repairing soft actuator, the number of connectors of the self-repairing soft actuator is finally set to 2.

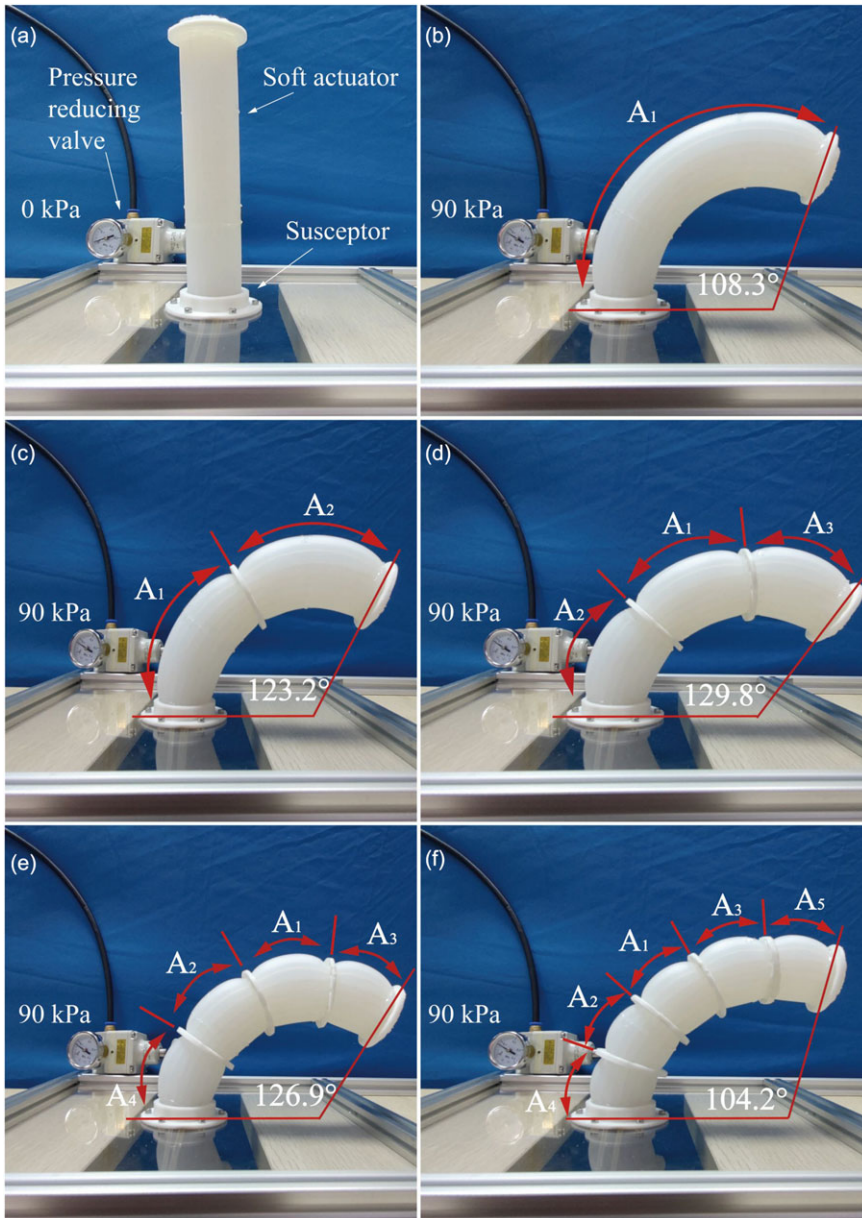


Figure 5. Bending experiment with different number of connectors installed. (a) Initial state. The soft actuator is fixed on the susceptor. (b–f) The inflation pressure is 90 kPa. The bending experiment is carried out when different numbers of connectors are installed.

3. Self-repairing principle

The self-repairing material used in this novel self-repairing soft actuator is different from other self-repairing materials. We use starch-based biomaterial particles to repair the soft actuator, as shown in Fig. 6(a).

For this self-repairing soft actuator, the total repair time T is equal to the heating time t_h , feeding time t_f , and cooling time t_c . The total repair time T , heating time t_h , and cooling time t_c are

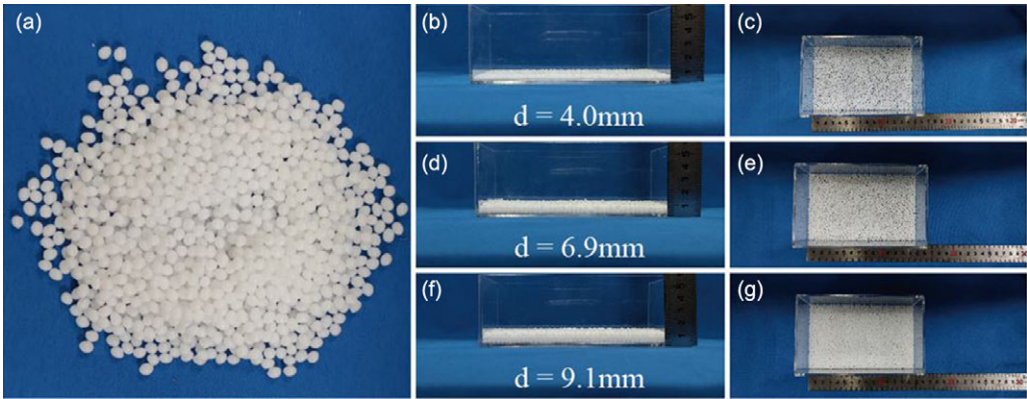


Figure 6. Self-repairing material particles and them with different layers.

$$\begin{aligned}
 T &= t_h + t_c + t_f = \frac{\kappa_h m \sigma}{P_{\text{wire}} l_{\text{wire}}} + \kappa_c m \sigma + t_f \\
 &= \left(\frac{\kappa_h R_{\text{wire}}}{U_{\text{wire}}^2} + \kappa_c \right) m \sigma + t_f, \tag{7}
 \end{aligned}$$

where m is the quality of self-repairing materials used in the self-repairing process, and σ is the repair material thickness. P_{wire} is the power of the heating wire, and l_{wire} is the length of the heating wire. U_{wire} is the heating voltage, and R_{wire} is the heating wire resistance. The environmental factor κ_h is the heating environment coefficient and κ_c is the cooling environment coefficient. The main factors affecting the environmental coefficient are wind speed, room temperature, the heating set temperature, and the thermal conductivity of the contact surface.

For the self-repairing soft actuator, the heating voltage U_{wire} , the length of the heating wire l_{wire} , and the heating wire resistance R_{wire} are fixed. For the determined working environment, the heating environment coefficient κ_h and cooling environment coefficient κ_c are also determined. Therefore, the main factors affecting the heating time and cooling time are the quality and the thickness of the repair material. For the self-repairing soft actuator, the actuator size is determined. Therefore, the thicker the repair material, the higher the quality of the repair material. Therefore, it is important to determine the thickness of the repair material for the repair time.

For the self-repairing soft actuator, the thicker the repair material, the better the repair effect, but the repair time will increase. Therefore, we carried out tensile experiments on repair materials with different thicknesses after heating. As shown in Fig. 6(b)–(g), we tested the repair materials with the thickness of one layer of particles (4.0 mm), two layers of particles (6.9 mm), and three layers of particles (9.1 mm).

After the self-repairing materials are heated, melted, and cooled, their thickness will change. The thickness is 2.3 mm for one layer of particles, 4.1 mm for two layers of particles, and 5.5 mm of three layers for particles after cooling. The tensile test machine (Zwick/Roell Z050) is used to carry out tensile test on self-repairing materials with different thickness and the results are shown in Fig. 7.

As shown in Fig. 7(a), the stress–strain curve of the self-repairing materials remains basically unchanged under different thicknesses. The elastic deformation remains unchanged until the deformation reaches 10% and the stress can reach 15 MPa. Then the self-repairing material starts plastic deformation in the tensile state, and the deformation variable can reach more than 11 times of the original length of the self-repairing materials. As shown in Fig. 7(b), the tensile force that the self-repairing materials can bear varies greatly under different thickness. When the material thickness is 2.3, 4.1, and 5.5 mm, the maximum tensile force within the elastic deformation range is 244.25, 489.42, and 665.41 N, and the final breaking tensile force reaches 368.03, 659.14, and 881.74 N. It can be found that with the increase of thickness, the hardness of the material also increases, and the force it can bear is also larger.

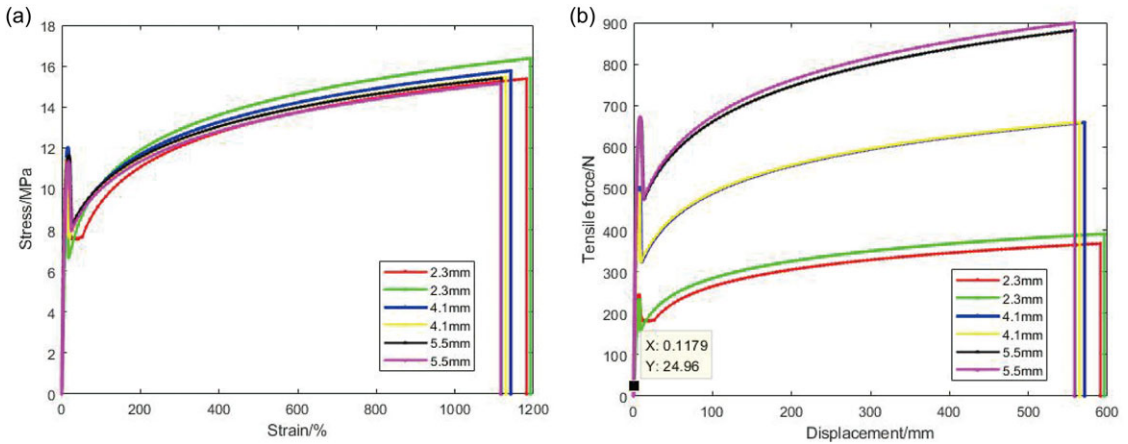


Figure 7. Tensile curves under different thicknesses. (a) Tensile stress–strain curves of self-repairing materials with different thicknesses. (b) Tensile force–displacement curves of self-repairing materials with different thickness.



Figure 8. Force test bench for bending of the self-repairing soft actuator.

For the self-repairing soft actuator, the load evenly distributed on the inner wall of the inflation chamber will be generated when it is bent. The repaired soft actuator requires that the repair position shall not bend and deform to maintain the tightness of the damaged position. Therefore, the repaired material layer should be able to withstand the force generated by the bending of the self-repairing soft actuator without large deformation. As shown in Fig. 8, the self-repairing soft actuator during bending is tested and it is found that the maximum force generated during bending is 24.96 N. Corresponding to Fig. 7(b), it is found that when the tensile force of the two-layer material thickness (4.1 mm) is 24.96 N, its deformation is 0.1179 mm. Under this deformation, the repair position of the self-repairing soft actuator will not be damaged. However, in the actual loading process, it is difficult to achieve uniform distribution of self-repairing material particles. If a layer of particles is used for repairing, the thickness of the damaged position may be less than 2.3 mm after feeding and repairing. Therefore, we decided to use repair

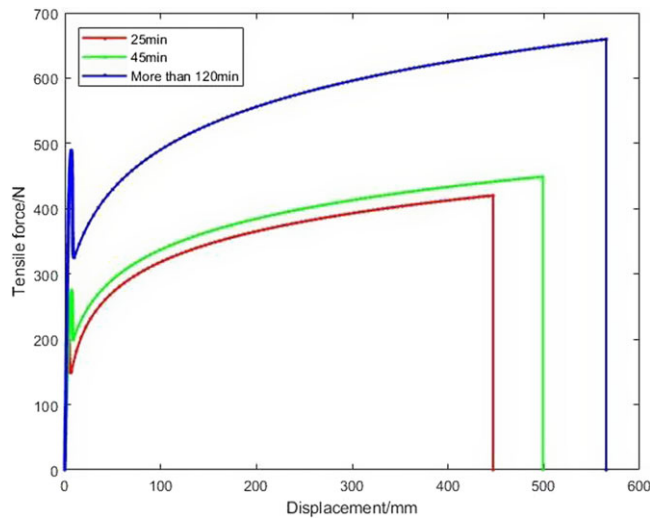


Figure 9. Tensile curves of self-repairing materials under different cooling times.

materials with a thickness of two-layer material thickness (6.9 mm) in the self-repairing process of the self-repairing soft actuator.

During the cooling process, the hardness of the self-repairing material will change with cooling time. When the hardness h of the self-repairing material can ensure that the repair part of the actuator is inflated without air leakage, the actuator can work normally. It is assumed that the hardness of the material after cooling is $H (H \geq h)$. Therefore, the tensile properties of the self-repairing material under different cooling times are tested, as shown in Fig. 9. The experiment is carried out with the self-repairing material of two-layer particles. The cooling times of the self-repairing material are 25 min, 45 min, and more than 120 min (complete cooling, respectively).

As shown in Fig. 9, with the change of cooling time, the maximum tensile force of the self-repairing material in the range of elastic deformation changes. At the same time, the maximum tension and displacement of the self-repairing material will also change. When the cooling time is 25 min, 45 min, and more than 120 min, the maximum tensile force within the elastic deformation range is 198.82, 274.75, and 489.42 N, the maximum tensile force at fracture is 420.22, 449.06, and 659.59 N, and the fracture displacement is 447.2, 499.1, and 565.3 mm. The tensile test results of self-repairing materials with different thickness and cooling time are shown in Tables II and III.

4. Self-repairing experiment and effect

4.1. Self-repairing experiment

Self-repairing experiment refers to the process of detecting and repairing the damaged position when the soft actuator is damaged. The performance of the self-repairing soft actuator can be reflected in two aspects [47]:

- Self-repairing time T
- Self-repairing efficiency η

For the self-repairing soft actuator, the restoration rate is unstable for two reasons:

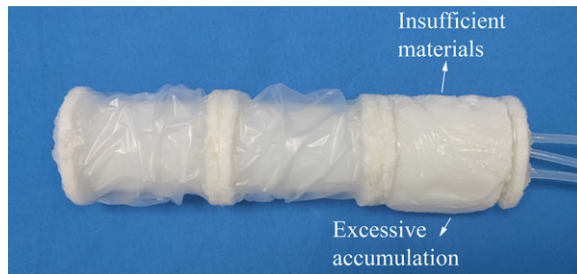
1. The heating time of starch-based biomaterials is insufficient during the self-repairing process. If the heating time is insufficient, the starch-based biomaterial cannot be completely melted,

Table II. Tensile test results of self-repairing materials with different thickness.

Self-repairing material thickness	Maximum tensile force within the elastic deformation range	Final breaking tensile force
2.3 mm	244.25 N	368.03 N
4.1 mm	489.42 N	659.14 N
5.5 mm	665.41 N	881.74 N

Table III. Results of overloading for three experimental setups.

Cooling time	Maximum tensile force within the elastic deformation range	Final breaking tensile force
25 min	198.82 N	420.22 N
45 min	274.75 N	449.06 N
120 min	489.42 N	659.59 N

**Figure 10.** Problems occurred in the self-repairing process of the self-repairing soft actuator.

and the bonding area between the starch-based biomaterial and the silicone rubber body will be smaller than that under normal conditions.

- Excessive heating. It takes quite a long time (more than 15 min at 90°C) for starch-based biomaterials to turn into liquid. Due to the long heating time, starch-based biomaterials began to flow under the influence of gravity. This leads to excessive accumulation of starch-based biomaterials in some positions, which increases the stiffness of the self-repairing soft actuator and affects the working performance of the soft actuator after self-repairing. At the same time, the starch-based biomaterials in another part are insufficient, which reduces the fracture strength of the starch-based biomaterials after the self-repairing of the soft actuator and reduces the self-repairing efficiency η .

As shown in Fig. 10, the starch-based biomaterial has insufficient materials on the upper side and excessive accumulation on the lower side during the self-repairing process.

Considering the excessive heating and insufficient heating of the self-repairing soft actuator during the self-repairing process, and through the test of starch-based biomaterials, it is finally determined to use two layers of repair material particles to repair the actuator. The mass of the repair material used is 40 g, the repair time is about 80 min, and the repair effect is tested. When the inflation pressure of the soft actuator is 90 kPa, we used tweezers to destroy the inflation chamber of the soft actuator, as shown in Fig. 11. This kind of damage is caused by penetrating a sharp object. It produced a pore and caused rupture and air leakage. After the air chamber is damaged, the soft actuator cannot bend normally.

By determining the damaged position of the air chamber, we rotate the connector at the corresponding position. Then, the self-repairing material enters the actuator enclosure from the end of the actuator

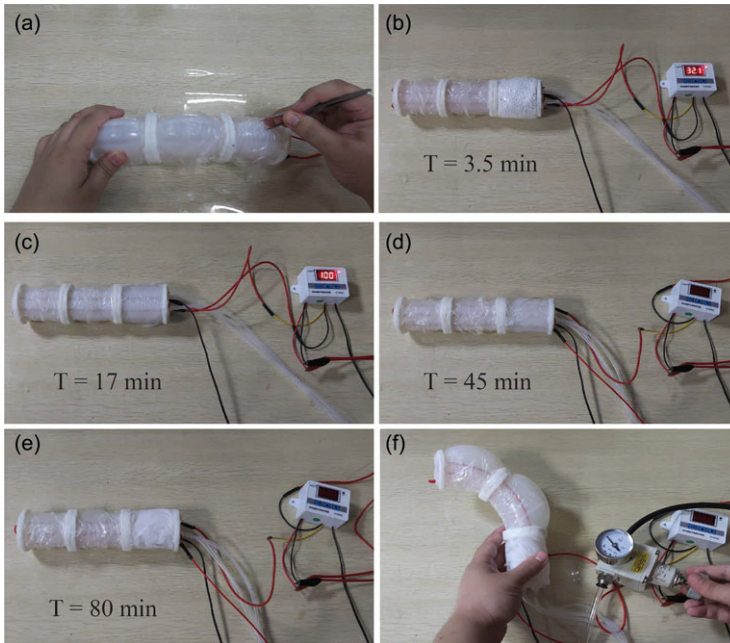


Figure 11. The self-repairing process of the self-repairing soft actuator. (a) Damage the actuator during inflation. (b) The self-repairing soft actuator with the self-repairing time of 3.5 min. (c) The self-repairing soft actuator with the self-repairing time of 17 min. At this time, the self-repairing material heating is completed. (d) The self-repairing soft actuator with the self-repairing time of 45 min. (e) The self-repairing soft actuator with the self-repairing time of 80 min. At this time, the self-repairing material is completely cooled. (f) Inflation test of the damaged air chamber of the self-repairing soft actuator.

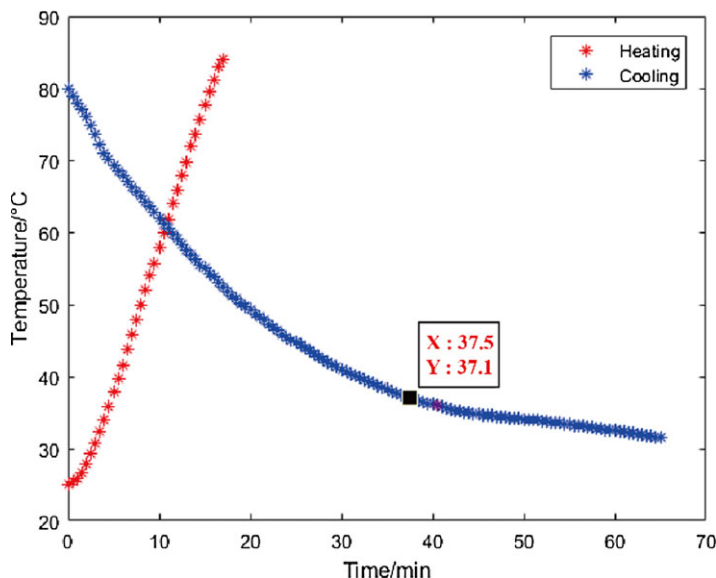


Figure 12. Self-repairing heating and cooling process of the self-repairing soft actuator.

Table IV. Comparison of the self-repairing soft actuator test before and after self-repairing.

	Maximum bending force	Maximum bending angle
Before self-repairing	24.96 N	129.8°
After self-repairing	21.85 N	108.2°
Variation	12.4%	16.6%

Table V. Comparison of the self-repairing time of other self-repairing soft actuators.

	Self-repairing time
This paper	≈1.3 h
Niu et al. [48]	> 8 h
Wang et al. [49]	> 6 h
Zhang et al. [50]	> 12 h
Cao et al. [51]	> 24 h

and quickly reaches the damaged area. When the self-repairing material reaches the damaged area completely, the heating line starts heating, as shown in Fig. 11. After heating for 17 min, it can be observed that the self-repairing material has completely melted and wrapped outside the damaged position of the actuator. At this time, the heating wire will automatically cut off the power supply and start cooling the self-repairing material. Considering the environmental factors, the cooling time is about 65 min. After cooling, the self-repairing material changes from colorless to white and from fluid to solid. The self-repairing material completes the self-repairing process and has completely wrapped the damaged position of the self-repairing soft actuator, as shown in Fig. 11(e). Then we inflate and test the self-repairing soft actuator. It is found that when the inflation pressure is 90 kPa, the self-repairing soft actuator can complete bending, as shown in Fig. 11(f).

The self-repairing heating and cooling process of the soft actuator is shown in Fig. 12. The heating speed is relatively balanced. The cooling speed changes more and more slowly with time. It takes 37.5 min to cool down from 80 to 37°C. And it takes 27.5 min to fall from 37 to 31.5°C. For the cooling process, the cooling rate from above 80 to 37°C is 1.15°C/min. However, in this process, the self-repairing material is still in the fluid state, and the required self-repairing effect cannot be achieved at this time. From 37°C, the self-repairing material quickly changes from liquid to solid, but the process cools slowly at a rate of 0.2°C/min.

4.2. Self-repairing effect

We test the bending force and the bending angle of the self-repairing soft actuator before and after self-repairing. Before self-repairing, the maximum bending force of the self-repairing soft actuator is 24.96 N and the bending angle is 129.8°. After self-repairing, the maximum bending force of the self-repairing soft actuator is 21.85 N and the bending angle is 108.2°, as shown in Table IV. The maximum bending angle of the self-repairing soft actuator is reduced by 16.6% and the maximum bending force of the self-repairing soft actuator is reduced by 12.4%, which has little impact on the work of the self-repairing soft actuator.

Compared with other self-repairing soft actuators, this novel self-repairing soft actuator has faster repair process and higher efficiency, as shown in Table V. In addition, the whole process can realize remote control and maintenance.

5. Conclusion

In this paper, a pneumatic self-repairing soft actuator is constructed. It consists of three parts: driving element, heating element, and repair element. The driving element completes the locomotion of the self-repairing soft actuator. The heating element and the repair element complete the self-repairing function of the self-repairing soft actuator. Through the finite element analysis of the self-repairing soft actuator, the structural optimization model of the self-repairing soft actuator is established. Through the structural optimization model, the repair components of the self-repairing soft actuator are finally divided into three sections. The self-repairing time model of the self-repairing soft actuator is established. The influences of different factors on the self-repairing effect and the self-repairing time are analyzed. The self-repairing scheme of the self-repairing soft actuator is determined. The repair effect of the self-repairing soft actuator is verified by experiments. According to the experiment, when the actuator is not damaged, the bending angle of the self-repairing soft actuator can reach 129.8° , and the bending force can reach 24.96 N. When the repair is completed, the bending angle of the self-repairing soft actuator can reach 108.2° , and the bending force can reach 21.85 N. After the self-repairing process, the self-repairing soft actuator can continue to work.

By optimizing the self-repairing scheme, it is determined that the shortest time of the self-repairing process is 83 min. Compared with other self-repairing soft actuators, it greatly reduces the repair time of the actuator and improves the repair efficiency of the soft actuator. Because the bending angle and the bending force of the self-repairing soft actuator are large, it can be used in crawling or grasping soft robots. Future work will focus on the sensing detection of the soft actuator and its security improvement in different environments.

Author's contributions. Zhaoyu Liu designed and manufactured a pneumatic self-repairing soft actuator and completed the modeling and experimental part. Yuxuan Wang contributed significantly to analysis and manuscript preparation. Shaoke Yuan performed the data analyses. Yanqiong Fei helped perform the analysis with constructive discussions.

Financial support. This work was supported by National Key technologies research and development program of China (No.2022YFB4703202), Institute of Medical Robotics of Shanghai Jiao Tong University under Grant No. IMR2019KY01, National Natural Science Foundation of China under Grant No. 51875335, Project No. 2021Szvup078, TMSK-2021-110.

Conflicts of interest. The authors declare no conflicts of interest exist.

Ethical approval. Not applicable.

References

- [1] F. Chen and M. Y. Wang, "Design optimization of soft robots: A review of the state of the art," *IEEE Robot. Autom. Mag.* **27**(4), 27–43 (2020).
- [2] J. Guo, K. Elgeneidy, C. Xiang, N. Lohse, L. Justham and J. Rossiter, "Soft pneumatic grippers embedded with stretchable electroadhesion," *Smart Mater. Struct.* **27**(5), 055006 (2018).
- [3] Z. Liu, Y. Wang, J. Wang, Y. Fei and Q. Du, "An obstacle-avoiding and stiffness-tunable modular bionic soft robot," *Robotica* **40**(8), 2651–2665 (2022).
- [4] D. Zhou, W. Zuo, X. Tang, J. Deng and Y. Liu, "A multi-motion bionic soft hexapod robot driven by self-sensing controlled twisted artificial muscles," *Bioinspir. Biomim.* **16**(4), 045003 (2021).
- [5] X. Yang, R. Tan, H. Lu and Y. Shen, "Starfish inspired milli soft robot with omnidirectional adaptive locomotion ability," *IEEE Robot. Autom. Lett.* **6**(2), 3325–3332 (2021).
- [6] H. Q. Abdulrab, I. N. A. M. Nordin, M. R. M. Razif and A. A. M. Faudzi, "Snake-like soft robot using 2-chambers actuator," *J. Electr. Electron. Eng.* **17**(1), 34–40 (2018).
- [7] Z. Liu, Y. Wang and Y. Fei, "Soft Pipe-Climbing Robot for Vertical Creeping Locomotion," *2021 27th International Conference on Mechatronics and Machine Vision in Practice (M2VIP)*, IEEE (2021, November) pp. 316–321.
- [8] Y. Yang, M. Zhang, D. Li and Y. Shen, "Graphene-based light-driven soft robot with snake-inspired concertina and serpentine locomotion," *Adv. Mater. Technol.* **4**(1), 1800366 (2019).
- [9] H. Jin, E. Dong, M. Xu, C. Liu, G. Alici and Y. Jie, "Soft and smart modular structures actuated by shape memory alloy (SMA) wires as tentacles of soft robots," *Smart Mater. Struct.* **25**(8), 085026 (2016).

- [10] D. Niu, W. Jiang, G. Ye, B. Lei, F. Luo, H. Liu and B. Lu, "Photothermally triggered soft robot with adaptive local deformations and versatile bending modes," *Smart Mater. Struct.* **28**(2), 02LT01 (2019).
- [11] C. Lee, M. Kim, Y. J. Kim, N. Hong, S. Ryu, H. J. Kim and S. Kim, "Soft robot review," *Int. J. Control. Autom. Syst.* **15**(1), 3–15 (2017).
- [12] C. Yin, F. Wei, S. Fu, Z. Zhai, Z. Ge, L. Yao, M. Jiang and M. Liu, "Visible light-driven jellyfish-like miniature swimming soft robot," *ACS Appl. Mater. Interfaces* **13**(39), 47147–47154 (2021).
- [13] Q. Wu, X. Yang, Y. Wu, Z. Zhou, J. Wang, B. Zhang, Y. Luo, S. A. Chepinskiy and A. A. Zhilenkov, "A novel underwater bipedal walking soft robot bio-inspired by the coconut octopus," *Bioinspir. Biomim.* **16**(4), 046007 (2021).
- [14] F. Lamping, R. Seis and K. M. de Payrebrune, "On the motion of a snake-like soft robot," *PAMM* **20**(1), e202000037 (2021).
- [15] R. K. Katzschmann, A. D. Marchese and D. Rus, "Hydraulic Autonomous Soft Robotic Fish for 3D Swimming," *In: Experimental Robotics*, (Springer, Cham, 2016) pp. 405–420.
- [16] Y. Li, T. Ren, Y. Li, Q. Liu and Y. Chen, "Untethered-bioinspired quadrupedal robot based on double-chamber pre-charged pneumatic soft actuators with highly flexible trunk," *Soft Robot.* **8**(1), 97–108 (2021).
- [17] G. Gu, J. Zou, R. Zhao, X. Zhao and X. Zhu, "Soft wall-climbing robots," *Sci. Robot.* **3**(25), eaat2874 (2018).
- [18] R. H. Ewoldt, "Extremely soft: Design with rheologically complex fluids," *Soft Robot.* **1**(1), 12–20 (2014).
- [19] T. Gao, D. Li, G. Jin, H. Liang and R. Yang, "Discrete Element Simulation of Mechanics Properties of Single Edge Notched Hydrogel-A New Material for Soft Robot and Sensor," *2018 WRC Symposium on Advanced Robotics and Automation (WRC SARA)*, IEEE (2018) pp. 96–101.
- [20] F. Jiang, Z. Zhang, X. Wang, G. Cheng, Z. Zhang and J. Ding, "Pneumatically actuated self-healing bionic crawling soft robot," *J. Intell. Robot. Syst.* **100**(2), 445–454 (2020).
- [21] D. G. Bekas, K. Tsirka, D. Baltzis and A. S. Paipetis, "Self-healing materials: A review of advances in materials, evaluation, characterization and monitoring techniques," *Compos. Part B Eng.* **87**, 92–119 (2016).
- [22] R. S. Trask, I. P. Bond and C. O. A. Semprimoschnig, "Self-Healing of Composite Structures in a Space Environment," *ICCM15-15th International Conference on Composite Materials Proceedings*, Durban (2006, September).
- [23] A. Cuvellier, A. Torre-Muruzabal, G. Van Assche, K. De Clerck and H. Rahier, "Selection of healing agents for a vascular self-healing application," *Polym. Test.* **62**, 302–310 (2017).
- [24] H. Ullah, K. S. Qureshi, U. Khan, M. Zaffar, Y. J. Yang, N. E. Rabat, M. I. Khan, S. Saqib, A. Mukhtar, S. Ullah, M. Mubashir, A. Bokhari, W. S. Chai, K. W. Chew, P. L. Show, "Self-healing epoxy coating synthesis by embedding of metal 2-methyl imidazole and acetylacetonate complexes with microcapsules," *Chemosphere* **285**, 131492 (2021).
- [25] F. Herbst, D. Döhler, P. Michael and W. H. M. Binder, "Rapid Commun. 3/2013," *Macromol. Rapid Commun.* **34**(3), 197–197 (2013).
- [26] G. M. van Gemert, J. W. Peeters, S. H. Söntjens, H. M. Janssen and A. W. Bosman, "Self-healing supramolecular polymers in action," *Macromol. Chem. Phys.* **213**(2), 234–242 (2012).
- [27] H. Zhang, S. Yang, Z. Yang, D. Wang, J. Han, C. Li, C. Zhu, J. Xu and N. Zhao, "An extremely stretchable and self-healable supramolecular polymer network," *ACS Appl. Mater. Interfaces* **13**(3), 4499–4507 (2021).
- [28] J. Dahlke, S. Zechel, M. D. Hager and U. S. Schubert, "How to design a self-healing polymer: General concepts of dynamic covalent bonds and their application for intrinsic healable materials," *Adv. Mater. Interfaces* **5**(17), 1800051 (2018).
- [29] N. Yuan, L. Xu, H. Wang, Y. Fu, Z. Zhang, L. Liu, C. Wang, J. Zhao and J. Rong, "Dual physically cross-linked double network hydrogels with high mechanical strength, fatigue resistance, notch-insensitivity, and self-healing properties," *ACS Appl. Mater. Interfaces* **8**(49), 34034–34044 (2016).
- [30] T. P. Huynh and H. Haick, "Self-healing, fully functional, and multiparametric flexible sensing platform," *Adv. Mater.* **28**(1), 138–143 (2016).
- [31] X. Y. Jia, J. F. Mei, J. C. Lai, C. H. Li and X. Z. You, "A highly stretchable polymer that can be thermally healed at mild temperature," *Macromol. Rapid Commun.* **37**(12), 952–956 (2016).
- [32] J. Liu, C. S. Y. Tan, Z. Yu, N. Li, C. Abell and O. A. Scherman, "Tough supramolecular polymer networks with extreme stretchability and fast room-temperature self-healing," *Adv. Mater.* **29**(22), 1605325 (2017).
- [33] Z. G. Joey, A. A. Calderón and N. O. Pérez-Arancibia, "An Earthworm-Inspired Soft Crawling Robot Controlled by Friction," *2017 IEEE International Conference on Robotics and Biomimetics (ROBIO)*, IEEE (2017, December) pp. 834–841.
- [34] Y. Li, S. Chen, M. Wu and J. Sun, "All spraying processes for the fabrication of robust, self-healing, superhydrophobic coatings," *Adv. Mater.* **26**(20), 3344–3348 (2014).
- [35] C. Laschi, B. Mazzolai and M. Cianchetti, "Soft robotics: technologies and systems pushing the boundaries of robot abilities," *Sci. Robot.* **1**(1), eaah3690 (2016).
- [36] S. J. Garcia, "Effect of polymer architecture on the intrinsic self-healing character of polymers," *Eur. Polym. J.* **53**, 118–125 (2014).
- [37] S. Terryn, J. Brancart, D. Lefeber, G. Van Assche and B. Vanderborght, "Self-healing soft pneumatic robots," *Sci. Robot.* **2**(9), eaan4268 (2017).
- [38] W. M. Xu, M. Z. Rong and M. Q. Zhang, "Sunlight driven self-healing, reshaping and recycling of a robust, transparent and yellowing-resistant polymer," *J. Mater. Chem. A* **4**(27), 10683–10690 (2016).
- [39] R. Fu, Y. Guan, C. Xiao, L. Fan, Z. Wang, Y. Li, Y. Li, P. Yu, L. Tu, G. Tan, J. Zhai, L. Zhou, C. Ning, "Tough and highly efficient underwater self-repairing hydrogels for soft electronics," *Small Methods* **6**(5), 2101513 (2022).
- [40] S. K. Tabrizian, F. Sahraeezartamar, J. Brancart, E. Roels, P. Ferrentino, J. Legrand, G. V. Assche, B. Vanderborght and S. Terryn, "A healable resistive heater as a stimuli-providing system in self-healing soft robots," *IEEE Robot. Autom. Lett.* **7**(2), 4574–4581 (2022).

- [41] T. E. Pillsbury, N. M. Wereley and Q. Guan, "Comparison of contractile and extensile pneumatic artificial muscles," *Smart Mater. Struct.* **26**(9), 095034 (2017).
- [42] A. Sedal, A. Wineman, R. B. Gillespie and C. D. Remy, "Comparison and experimental validation of predictive models for soft, fiber-reinforced actuators," *Int. J. Robot. Res.* **40**(1), 119–135 (2021).
- [43] Z. Chen, A. Zou, Z. Qin, X. Han, T. Li and S. Liu, "Modeling and fabrication of soft actuators based on fiber-reinforced elastomeric enclosures," *Actuators* **10**(6), 127 (2021).
- [44] A. Darmohammadi, H. R. Naeimi and M. Agheli, "Effect of Fiber Angle Variation on Bending Behavior of Semi-Cylindrical Fiber-Reinforced Soft Actuator," *International Design Engineering Technical Conferences and Computers and Information in Engineering Conference*, American Society of Mechanical Engineers, Vol. 51814, (2018, August) p. V05BT07A054.
- [45] M. Y. Wang, X. Wang and D. Guo, "A level set method for structural topology optimization," *Comput. Methods Appl. Mech. Eng.* **192**(1-2), 227–246 (2003).
- [46] O. H. Yeoh, "Some forms of the strain energy function for rubber," *Rubber Chem. Technol.* **66**(5), 754–771 (1993).
- [47] S. Miyake, S. Nagahama and S. Sugano, "Development of self-healing linear actuator unit using thermoplastic resin," *Adv. Robot.* **33**(23), 1235–1247 (2019).
- [48] P. Niu, N. Bao, H. Zhao, S. Yan, B. Liu, Y. Wu and H. Li, "Room-temperature self-healing elastomer-graphene composite conducting wires with superior strength for stretchable electronics," *Compos. Sci. Technol.* **219**, 109261 (2022).
- [49] Z. Wang, K. Zhang, Y. Liu, H. Zhao, C. Gao and Y. Wu, "Modified MXene-doped conductive organosilicon elastomer with high-stretchable, toughness, and self-healable for strain sensors," *Compos. Struct.* **282**, 115071 (2022).
- [50] Y. Zhang, M. Li, B. Qin, L. Chen, Y. Liu, X. Zhang and C. Wang, "Highly transparent, underwater self-healing, and ionic conductive elastomer based on multivalent ion-dipole interactions," *Chem. Mater.* **32**(15), 6310–6317 (2020).
- [51] Y. Cao, Y. J. Tan, S. Li, W. W. Lee, H. Guo, Y. Cai, C. Wang and B. C.-K. Tee, "Self-healing electronic skins for aquatic environments," *Nat. Electron.* **2**(2), 75–82 (2019).